JACS
JOURNAL OF THE AMERICAN CHEMICAL SOCIETY
Article
pubs.acs.org/JACS

Size-Dependent Catalytic Activity of Supported Vanadium Oxide Species: Oxidative Dehydrogenation of Propane

Xavier Rozanska, Remy Fortrie, and Joachim Sauer*

Institut für Chemie, Humboldt Universität zu Berlin, Unter den Linden 6, D-10099 Berlin, Germany

Supporting Information

ABSTRACT: Possible reaction pathways for the oxidative dehydrogenation of propane by vanadium oxide catalysts supported on silica are examined by density functional theory. Monomeric and dimeric vanadium oxide species are both considered and modeled by vanadyl-substituted silsesquioxanes. The reaction proceeds in two subsequent steps. In a first step, hydrogen abstraction from propane by a vanadyl (O═V) group yields a propyl radical bound to a HOV^{IV} surface site. Propene is formed by a second hydrogen abstraction, either at the same vanadia site or at a different one. V^{V}/V^{IV} redox cycles are preferred over V^{V}/V^{III} cycles. Under the assumption of fast reoxidation, microkinetic simulations show that the first step is rate-determining and yields Arrhenius barriers that are lower for dimers (114 kJ/mol at 750 K) than for monomers (124 kJ/mol). The rate constants predicted for a mixture of monomers and dimers are 14% larger (750 K) than for monomers only, although the increase remains within experimental uncertainty limits. Direct calculations of energy barriers also yield lower values for dimeric species than for monomeric ones. Reactivity descriptors indicate that this trend will continue also for larger oligomers. The size distribution of oligomeric species is predicted to be rather statistical. This, together with the small increase in the rate constants, explains that turnover frequencies observed for submonolayer coverages of vanadia on silica do not vary with the loading within the experimental uncertainty limits.

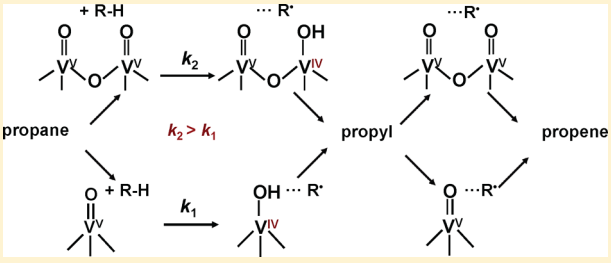

1. INTRODUCTION

Supported transition metal oxides are an important class of solid catalysts that are industrially used in selective oxygenation and oxidation processes of hydrocarbons. Much effort has been and is being spent on understanding the reaction mechanisms with the aim to improve the product selectivity while avoiding side reactions leading to formation of CO_x species.[1−4] Not less has been the effort spent on understanding the complex surface structure of the supported oxides. The prevailing picture includes different types of active species, ranging from monomeric over oligomeric to polymeric transition metal oxide clusters anchored on the surface of the supporting oxide, to nanocrystallites of the active component with the structure of the bulk transition metal oxide.[2,5−9] Activity and selectivity of such catalysts have been shown to change significantly when the support is varied for a given active oxide. This has tempted some scientists to conclude that the interphase oxygen atoms connecting the active oxide with the supporting oxide are actively involved in the elementary oxidation steps. An alternative interpretation is that the surface structure of the catalyst, e.g., the distribution of species of different size, may change with the support. To date, there is no experimental approach that would unequivocally allow for determining the size distribution of the active species on the surface. For very low loadings of the active component (of the order of one transition metal atom per nm^2 of support surface) the assumption is made that only monomeric species are present, but proving this appears difficult.[10,11] For example, it has been shown that V−O−V bonds, which would be absent in monomeric species, cannot be identified in IR or Raman spectra because of overlap with bands of the supporting oxide.[7] UV−vis absorption spectra are also not size-discriminating, although there is no doubt that the O 2p−V 3d charge transfer transitions will shift to lower energies with increasing particle size.[8,12]

Here, we use density functional theory (DFT) to provide information that cannot be easily obtained from experiments. We construct models for monomeric, dimeric, and polymeric supported species, and we examine them in comparison to surfaces of the bulk crystal. We study the reaction mechanisms that lead to the desired product, and for the crucial elementary steps, we can compare rates and activation barriers obtained for the active species of different size. In the present study we do this for the oxidative dehydrogenation (ODH) of propane to propene by vanadium oxides supported on silica. We find that the energy barriers are lower for dimeric species than for monomeric species and that this trend continues for larger species. Using DFT, we also compare the stabilities of vanadium oxide species of different size on silica. We find that there is almost no energetic preference for larger or smaller species. This means that, if we exclude kinetic phenomena, the

Received: March 30, 2014
Published: May 14, 2014

   dx.doi.org/10.1021/ja503130z | J. Am. Chem. Soc. 2014, 136, 7751−7761

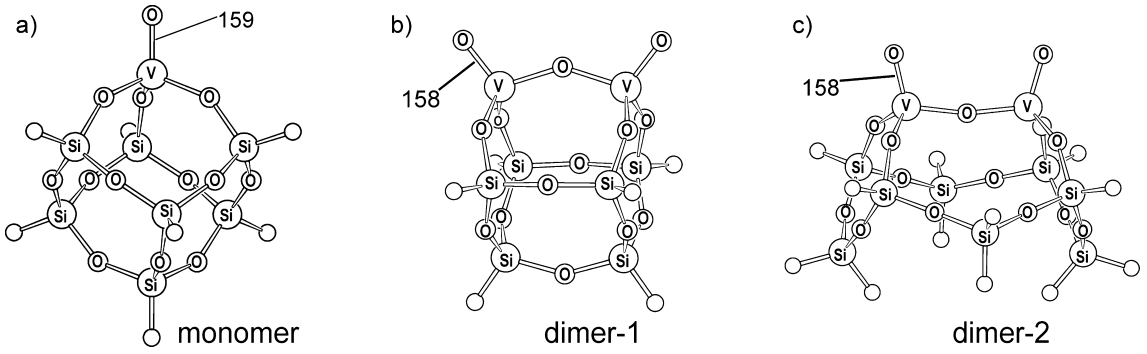

Figure 1. Models for monomeric and dimeric vanadium oxide species on silica. Distances are in pm.

size distribution of vanadium oxide species on silica surfaces will be largely statistical and that species of different size may contribute to the observed conversion of propane to propene.

We have chosen this reaction as example because oxidative dehydrogenation of small alkanes in general and of propane in particular is an exothermic route to small alkenes, from which many valuable products can be obtained in petrochemistry.[13−16] Not least, catalytic C−H bond activation by transition metal oxo bonds is of fundamental interest and studied also in homogeneous and enzymatic catalysis as well as in gas phase chemistry; see the literature for examples.[17−20]

Propane ODH is also becoming a reaction of reference for analyzing oxidation catalysis involving C−H bond activation.[21] Supported vanadium oxide catalysts have shown attractive ODH rates for alkanes in general and for propane in particular.[1,2,16,22] The dependence of alkene formation rates on the vanadia surface density has been studied for silica supports,[8,23−25] but also for alumina, titania, and zirconia supports.[6,8] Detailed kinetic studies showed that propene formation involves the activation of the secondary C−H bond in propane. Following Mars−van Krevelen, reoxidation of the catalyst is decoupled from propane activation and may involve both V^{+V}/V^{+IV} and/or V^{+V}/V^{+III} redox cycles. The elementary steps of the propane ODH are not known. Previously, we analyzed all possible reaction mechanisms for monomeric vanadium oxide species.[26] Similar studies have been made for the V_2O_5 (001) crystal surface,[27−29] for isolated V_4O_{10} clusters,[30] and for VO_2-exchanged MCM22 zeolites.[31] With regard to support effects, computational studies have been performed, e.g., on an epitaxial vanadia monolayer supported on a (001) anatase (TiO_2) surface,[32] and on anatase supported vanadium oxide monomers and dimers.[33]

Here, we examine the activity differences between dimeric and a monomeric vanadium oxide sites on silica. This results in a rather complex reaction network for which we perform microkinetic simulations with the aim of identifying dominant kinetic pathways. On this basis, we discuss how the ODH activity depends on the vanadia surface density in comparison to experimental data.

2. MODELS

We adopt polyhedral oligomeric silsesquioxanes as models for the amorphous silica support (Figure 1).[7,26,34] Replacing a Si−H moiety in the $H_8Si_8O_{12}$ silsesquioxane by vanadyl (V=O) yields the $O{=}VH_7Si_7O_{12}$ model for an isolated site (Figure 1, monomer). Replacing an increasing number of Si−H groups by V=O yields models for oligomeric vanadium oxide species, $(O{=}V)_nSi_{8-n}O_{12}H_{8-n}$. Up to n = 4, the models include silica sites on which vanadia is anchored. These models are representative of possible "monolayer" species at submonolayer coverage. The limiting case, V_8O_{20}, represents a vanadium oxide particle that is weakly interacting with the support. Its structure is different from bulk V_2O_5 crystallites,[35−37] and it does not represent V_2O_5 crystallites that are found on supported catalysts for vanadia loadings above 10 V atoms/nm^2.[6]

The model for a dimeric vanadium oxide site, $(O{=}V)_2H_6Si_6O_{12}$, is shown in Figure 1 (dimer-1). To check the effect of the local structure of the silica support on the activity, a second model is used for the dimeric site, which consists of two $O{=}VO_{3/2}$ units, four $H\text{-}SiO_{3/2}$ units and four $H_2SiO_{2/2}$ units (dimer-2 in Figure 1). In the dimer-2 model, the two vanadyl groups are almost parallel, whereas they point away from each other in the dimer-1 model.

3. METHODS

3.1. DFT Calculations. We apply density functional theory (DFT) with the hybrid B3LYP functional[38] and triple-ζ plus polarization basis sets (TZVP) on all atoms.[39] The Turbomole 5.7 code is employed.[40,41] B3LYP gives vanadium oxide structures and oxygen defect formation energies in good agreement with quantum chemical ab initio methods.[35] Unrestricted Kohn−Sham (UB3LYP) is used for systems with triplet and open-shell singlet spin states. The latter are treated within the broken-symmetry approach,[42] and spin-projected energies[43] for the low-spin (singlet) states are also obtained. All stationary points are characterized by frequency calculations.[44] All reported energies include zero-point vibrational contributions unless otherwise stated.

Classical transition state theory is used to calculate rate constants from the Gibbs free energies of transition structures (Ts), intermediates (Int), and hydrocarbon species in the gas phase separated from surface sites (S + hc). The partition functions for the gas phase species are calculated within the harmonic oscillator−rigid rotor−ideal gas approximation including vibrational, rotational, and translational degrees of freedom. As part of a solid body, the surface species Ts (transition structure), Int (intermediate), and S (surface site) do not have rotational or translational degrees of freedom. All N-6 internal degrees of freedom, including internal hindered rotations, are treated as harmonic vibrations. Since the corresponding mathematical expressions exist under several different forms, those that we used are gathered within the Supporting Information. Further details can also be found in the literature.[26]

3.2. Microkinetic Simulations. The reaction is considered to take place in a batch reactor with constant volume. The conditions of the plug flow experiments of Kondratenko et al.[25] are adopted: temperature = 750 K, volume = 98.2 mm^3, catalytic surface = 43.55 m^2, initial vanadium coverage = 0.5 nm^{-2}, initial pressure = 100 kPa with a propane:O_2:inert gas ratio of 40:40:20.

All reactive steps as well as adsorption and desorption steps obtained by DFT are considered; see Table S4a−c (Supporting Information) for the reactions included and the data used for the

dx.doi.org/10.1021/ja503130z | J. Am. Chem. Soc. 2014, 136, 7751−7761

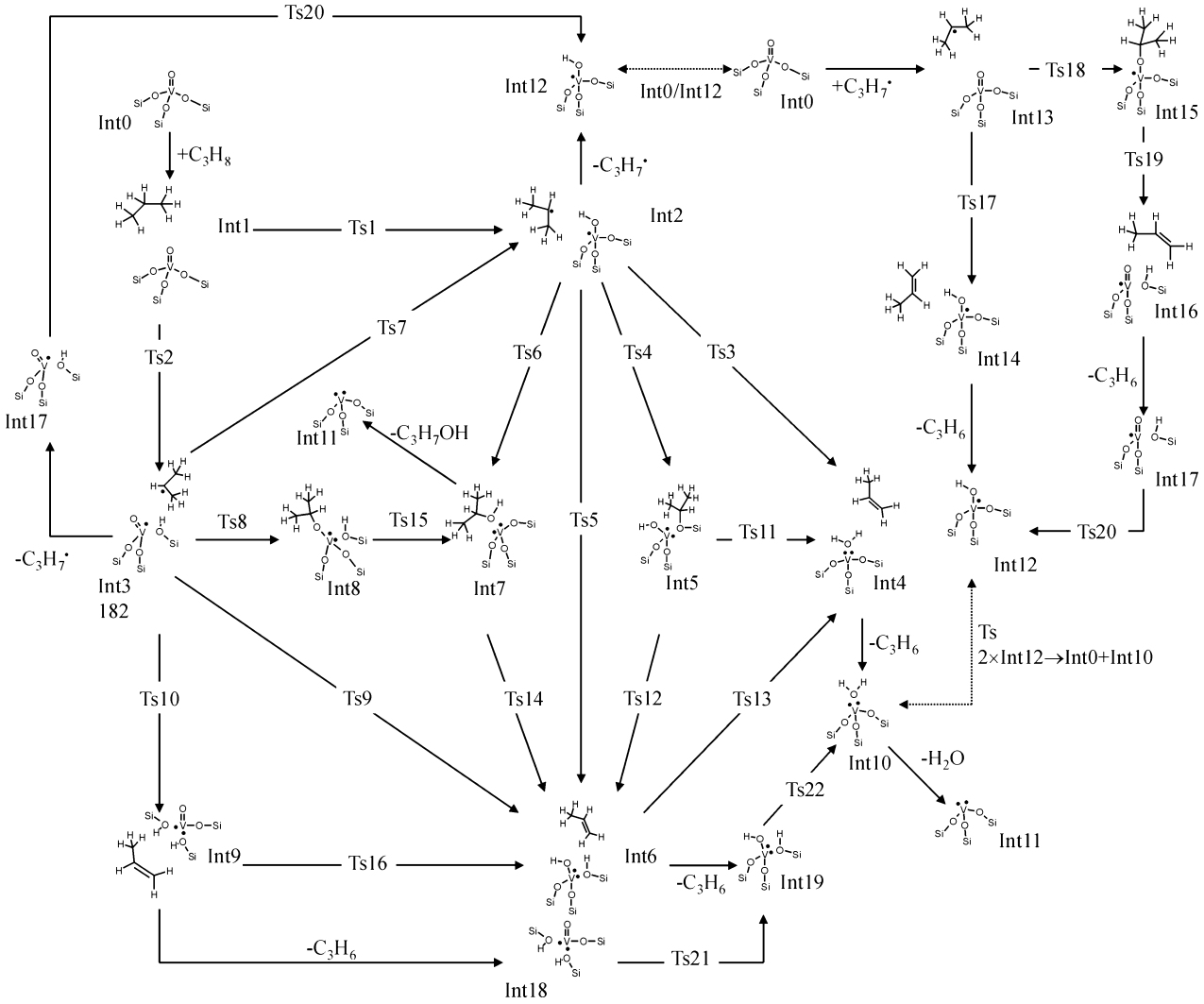

Figure 2. Reaction pathways in the oxidative dehydrogenation of propane by monomeric vanadium oxide active sites.[19] See Table S1 (Supporting Information) for the zero point and Gibbs free energies of the different structures.

individual steps. Reoxidation is assumed to occur along the processes listed in Table S4d (Supporting Information). All reoxidation reactions are assumed to be irreversible and nonactivated; i.e., the Gibbs free energy barrier is zero. The latter assumption is supported by a recent DFT study on the reoxidation of reduced vanadia sites.[45]

Note that intermediates with decoupled electron pairs are all considered both as triplets and open-shell singlets. The electronic energies of the latter are spin-projected energies, whereas vibrational contributions are calculated for the broken-symmetry potential energy surface. Both electronic states are being considered to be at equilibrium; see Supporting Information Table S4c. Note that all reactions starting from these intermediates and leading to triplet products start from triplet forms, whereas reactions leading to singlet products start from (broken symmetry) singlet forms.

To account for van der Waals interactions neglected in B3LYP, in the energy of all compounds with adsorbed propane, propyl, propene, or propanol, an energy correction of −37 kJ mol^{-1} has been added.[26,46]

The expressions used for calculating adsorption and desorption rates are provided, along with the necessary numerical material, within the Section S2 of the Supporting Information.

Finally, surface intermediates may exhibit several equivalent reactive sites. For example, in the case of Int0, propane can react onto three different lattice oxygen atoms and lead to three energetically equivalent, but orientationally different intermediates. These additional degrees of freedom have to be taken into account for kinetic simulations and are here considered through additional isomeric Gibbs free energies, G_{iso}, that are equal to $-k_BT\ln(Z_{iso})$, where Z_{iso} is the number of equivalent pathways or reactive centers. Note that 2D representations of reaction intermediates and transition structures may be misleading about the number of isomers that has to be considered. The Z_{iso} values used for the different isomers are given in Section S2.5 of the Supporting Information.

In Table S4a−d of the Supporting Information, Gibbs free reaction energies, Gibbs free energy barriers, and reaction rates for all reactions included in the simulation are collected. These values include van der Waals energy contributions and isomeric corrections.

Coupled differential equations are numerically solved in logarithmic time scale using Mathematica 5.2.[47] The backward differentiation formulas (BDF) algorithm is used, and each solution is converged at each point of the simulation up to the eighth decimal place.

4. RESULTS AND DISCUSSION

4.1. Reaction Mechanisms for Dimeric Vanadium Oxide Sites. Previously,[26] we found that ODH of propane on monomeric vanadium oxide sites proceeds via a diradical intermediate in two subsequent hydrogen abstraction steps and that barriers are lower if the second hydrogen abstraction occurs on a different, "unreacted" monomeric vanadia site. In the latter case, two $V^{IV}(d^1)$ species are reached at the end of the reaction instead of one $H_2O{\cdot}V^{III}(d^2)$ species.[48] This supposes

dx.doi.org/10.1021/ja503130z | J. Am. Chem. Soc. 2014, 136, 7751−7761

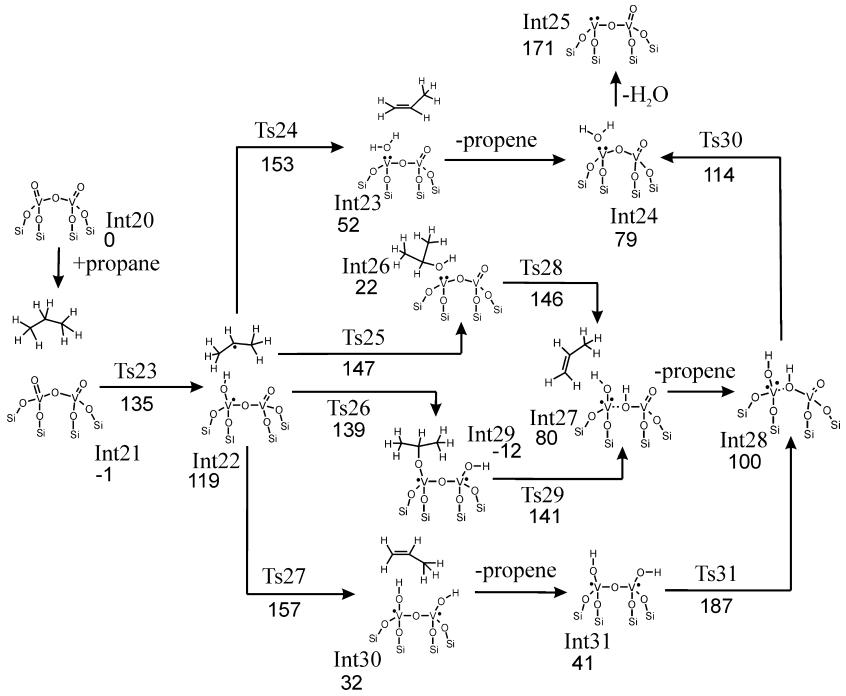

Figure 3. Reaction mechanisms in the oxidative dehydrogenation of propane by a dimeric vanadium oxide active site. The values are zero point energies in kJ/mol.

that $C_3H_7^\bullet$ formed by the first hydrogen abstraction desorbs from the $HOV^{IV}(d^1)$ site and readsorbs to an unreacted $O{=}V^{V}(d^0)$ species elsewhere. The second hydrogen atom is abstracted from $C_3H_7^\bullet$ by the oxygen of the vanadyl group. Figure 2 shows the dominant reaction pathways, and the energies are summarized in the Supporting Information, Table S1.

The reaction pathways for dimeric vanadium oxide sites (Figure 1) are shown in Figure 3, and the energies are reported in Table 1. The first step is propane adsorption to the active site (Int21). The adsorption energy is again underestimated because of the poor description of van der Waals interactions by B3LYP.[49] The vanadyl group abstracts a hydrogen atom from propane (Ts23), leading to $C_3H_7^\bullet$ (Int22). In the HOV group of Int22, vanadium has one electron in a d-state and is in the +IV oxidation state, i.e., $V^{IV}(d^1)$, whereas in the adjacent vanadyl group vanadium atom is still $V^{V}(d^0)$. Int22 is a biradical; its triplet and (open-shell) singlet states, Int22(t) and Int22(s), have similar energies.

We consider the four dominant reaction routes that further convert $C_3H_7^\bullet$ to C_3H_6. Two mechanisms are possible, hydrogen abstraction from $C_3H_7^\bullet$ (Ts24 and Ts27) leading directly to C_3H_6, and rebinding of $C_3H_7^\bullet$ to an oxygen atom of the vanadia cluster leading to isopropanol (Ts25) or isopropoxide (Ts26). The two reactions for each mechanism differ by the oxygen site involved, the $HOV^{IV}(d^1)$ group (Ts24, Ts25) or the $O{=}V^{V}(d^0)$ group (Ts26, Ts27). There is not much preference for either of them. For the HOV group the barrier for the hydrogen abstraction from $C_3H_7^\bullet$ is 4 kJ/mol lower and the barrier for $C_3H_7^\bullet$ attachment is 8 kJ/mol higher than for the O=V group. The $V^{IV}(d^1)/V^{IV}(d^1)$ products (Int29 and Int30) formed when the $O{=}V^{V}(d^0)$ group reacts are more stable than the $V^{III}(d^2)/V^{V}(d^0)$ products (Int23 and Int26) formed from the HOV group reacts.

The transition structures giving isopropoxide and isopropanol (Ts25 and Ts26) have lower energies than the transition

Table 1. Electronic Energies, E_{el}, Energies at 0 K, E_0, and Gibbs Free Energies at Temperature T (K) G_T, All in kJ/mol, for the Oxidative Dehydrogenation of Propane by Vanadium Oxide Dimers on Silica

system[a]	E_{el}	E_0	G_{600}	G_{800}
Int20 + C_3H_8(s)	0	0	0	0
Int21(s)	−1	−1	17	19
Int22(s)	131 (130)	119 (118)	182 (181)	197 (196)
Int22(t)	132	120	180	195
Int23(t)	57	52	109	123
Int24(t) + C_3H_6	87	79	62	53
Int25(t) + C_3H_6 + H_2O	188	171	73	38
Int26(t)	15	22	109	135
Int27(t)	87	80	125	134
Int28(t) + C_3H_6	112	100	81	71
Int29(t)	−12	−12	68	90
Int30(s)	42 (47)	32 (37)	88 (93)	100 (105)
Int30(t)	42	31	90	102
Int31(s) + C_3H_6	58 (63)	44 (49)	22 (27)	10 (15)
Int31(t) + C_3H_6	55	41	24	14
Ts23(s)	154 (141)	135 (122)	224 (211)	250 (237)
Ts24(t)	171	153	225	245
Ts25(t)	161	147	208	223
Ts26(t)	153	139	202	219
Ts27(s)	183 (188)	161 (166)	230 (235)	249 (254)
Ts27(t)	179	157	227	245
Ts28(t)	161	146	240	268
Ts29(t)	159	141	232	259
Ts30(t) + C_3H_6	133	114	108	105
Ts31(t) + C_3H_6	212	187	174	167

[a]The letters t and s in parentheses stand for triplet and singlet electronic states, respectively. In parentheses: spin-projected energies.

dx.doi.org/10.1021/ja503130z | J. Am. Chem. Soc. 2014, 136, 7751−7761

structures yielding directly C_3H_6 (Ts24 and Ts27). However, when the free energies at reaction temperature are considered, the opposite is true, which was also found for monomeric vanadium oxide sites.[26]

The elimination of C_3H_6 from surface isopropanol and isopropoxide, Int26 and Int29, via Ts28 and Ts29 yields the same intermediate Int27. We do not consider pathways leading to alternative intermediates with hydrogen attached to oxygen in V−O−Si sites as shown in Figure 4, because they have 11−33 kJ/mol higher energies than Int27.

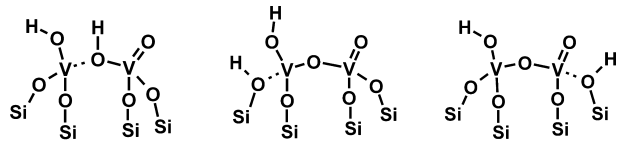

Figure 4. Int28 and isomers with hydrogen attached to different bridging oxygen atoms. The electronic energies in kJ/mol are given with respect to Int20 + C_3H_8(s) (Table 1).

From Int23, Int27, and Int30, C_3H_6 can desorb, which restores the six degrees of translation and rotation of the molecule and gives a very large free energy gain at reaction temperature (600 to 800 K). Although the interaction between H_2O and the $V^{III}(O-)_3$ site in Int24 is around 100 kJ/mol, desorption of H_2O (see Int25) becomes possible at reaction temperature because of the entropy gain. However, at such temperatures the more stable product is Int31, which involves a $V^{IV}(d^1)/V^{IV}(d^1)$ pair. Although hydrogen migrations through Ts30 and Ts31 have to pass high energy barriers (the energy of Ts31 is the highest of all in the reaction scheme), free energies in Table 1 show that this process is fast compared to the rate-determining step. This implies that after C_3H_6 has been formed from C_3H_8, the reduced vanadium oxide will mainly exist as $V^{IV}(d^1)$, i.e., the catalyst undergoes a $V^{V}(d^0)/V^{IV}(d^1)$ redox cycle.

So far, we considered the reaction pathways on the triplet potential energy surface. For monomeric vanadium oxide species, the reaction on the singlet potential energy surface is unambiguously more difficult than on the triplet surface after $C_3H_7^{\bullet}$ and HO-$V^{IV}(d^1)$ is reached.[26] In contrast, for the reaction with a dimeric vanadium oxide site, all structures from the beginning until the end possess virtually the same energy on the triplet and singlet potential energy surfaces, as the two electrons transferred with the hydrogen atoms from C_3H_8 can stay apart in d-states of the two different vanadium atoms. To illustrate this point, Int22, Ts27, Int30, and Int31 are optimized both on the broken-symmetry and triplet potential energy surfaces. The energies are shown in Table 1.

In the dimer-1 cluster model used for all the above calculations the two vanadyl groups are pointing away from each other (Figure 1). To examine the effect of the local structure of the silica support on the activity, we use the dimer-2 cluster model (Figure 1) in which the two vanadyl groups are parallel and recalculate the energies for one of the reaction pathways with this model (Table 2). For the dimer-2 model, the energies are systematically larger than for the dimer-1 model, up to 6 kJ/mol for transition structures and up to 10 kJ/mol for intermediates. For Int22 an even larger cage-like dimer-model has been considered (model 3a from the literature[7]) that has a similar parallel orientation of the vanadyl bonds as dimer-2 and that we call dimer-2*. The energies for Int22(s) are 131, 134, and 139 kJ/mol for dimer-1, dimer-2, and dimer-2*; i.e., the energies for all three models are within 9 kJ/mol. The precise local structure of the active site does not seem to have a strong effect on the activity of the catalyst. Table 2 also shows that deviations between dimer-1 and dimer-2 results are larger for Gibbs free energies and that dimer-2 results may not always be larger. For Ts23, Int22, Int30(s), they are smaller.

Table 2. Electronic Energies, E_{el}, Energies at 0 K, E_0, and Gibbs Free Energies at Temperature T (K) G_T, All in kJ/mol, for the Oxidative Dehydrogenation of Propane Obtained with the Dimer-2 Model[a]

system[b]	E_{el}	E_0	G_{600}	G_{800}
Int20 + C_3H_8(s)	0	0	0	0
Int21(s)	−1	−1	20 (+3)	24 (+5)
Ts23(s)	155 (+1)	136(+1)	212 (−12)	234 (−16)
Int22(s)	134 (+3)	122 (+3)	172 (−10)	183 (−14)
Int22(t)	136 (+4)	124 (+4)	194 (+14)	211 (+16)
Ts27(s)	188 (+5)	167 (+6)	246 (+19)	268 (+19)
Ts27(t)	182 (+3)	160 (+3)	245 (+5)	269 (+24)
Int30(s)	50 (+8)	40(+9)	87 (−1)	97 (−5)
Int30(t)	47 (+5)	37 (+6)	93 (+3)	105 (+3)

[a]In parentheses: Difference to the dimer-1 results (Table 1). [b]See Figure 1; the letters t and s in parentheses refer to triplet and singlet electronic states, respectively.

The two subsequent hydrogen abstractions can also take place on two different dimeric sites, yielding two V^{IV}/V^{V} species. Figure 5 shows the relevant transition structures, Ts32 − Ts34, and intermediates, Int32 − Int37. The energies are in Table 3. Compared to the reaction on one dimeric site, the reaction energy and the energy barrier decrease by 12 and 17 kJ/mol, respectively.

Figure 6 summarizes the different possibilities emerging from the first and second hydrogen abstraction to occur on a monomer or a dimer, and on the same site or a different site. Two subsequent hydrogen abstractions at the same monomeric site yielding vanadium(III) are clearly disfavored, whereas the other pathways will be competing as the free energies are all in a range of about 20 kJ/mol.

4.2. Comparison of Monomeric and Dimeric Species.

Comparison of the reaction energies and energy barriers for monomeric and dimeric species is made in Table 4. The energy barrier for the initial hydrogen abstraction is 9 kJ/mol lower for dimeric vanadium oxide species (Ts23) than for a monomeric species (Ts1). The reaction energy is 13 kJ/mol lower. The barrier for the second hydrogen abstraction is 26 kJ/mol lower for dimeric species (Ts24) than for monomeric species (Ts3) when leading to a $H_2O{\cdot}V^{III}(d^2)$ site. Subsequent hydrogen abstractions by two vanadyl sites yield two HOV^{IV} sites. If this happens on a dimeric vanadium oxide species, the energy barrier for the second hydrogen abstraction (Ts27) is 17 kJ/mol lower than for two isolated monomeric sites (Ts17). For two dimeric species (Ts32), the barrier further reduces by 35 kJ/mol. The corresponding changes of the reaction energies are 11 (Int30−Int14) and 28 kJ/mol (Int34−Int14). For the dimer-2 model very similar results are obtained.

These results provide evidence that reductions of energy barriers are always accompanied by corresponding changes of the reaction energies in accord with the Polanyi−Evans relation.[50] The latter strictly refers to the product that is directly reached from the transition structure, namely, Int22/

dx.doi.org/10.1021/ja503130z | J. Am. Chem. Soc. 2014, 136, 7751−7761

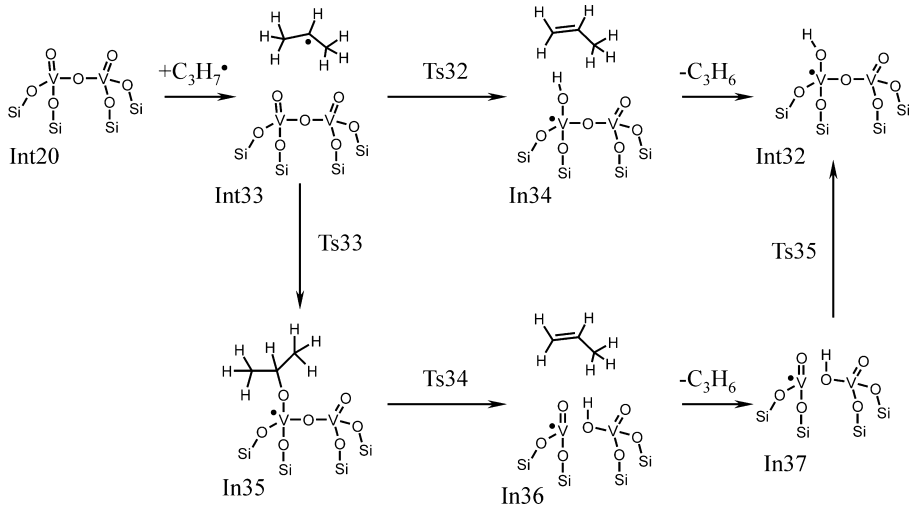

Figure 5. Reaction pathway of the hydrogen abstraction of $C_3H_7^•$ by dimer-1 (see Table 5).

Table 3. Electronic Energies, E_{el}, Energies at 0 K, E_0, and Gibbs Free Energies at Temperature T (K) G_T, All in kJ/mol, for the Oxidative Dehydrogenation of Propane by Two Dimeric Vanadium Oxide Species on Silica[a]

system[a]	E_{el}	E_{ZPE}	G_{600}	G_{800}
Int20 + Int20 + C_3H_8	0	0	0	0
Int20 + Int32 + $C_3H_7^•$	148	148	127	114
Int32 + Int33	144	129	180	191
Int32 + Ts32	161	140	216	237
Int32 + Int34	26	15	72	84
Int32 + Ts33	143	128	199	218
Int32 + Int35	−26	−26	55	80
Int32 + Ts34	140	122	214	241
Int32 + Int36	71	62	117	130
Int32 + Int37 + C_3H_6	99	86	67	57
Int32 + Ts35 + C_3H_6	198	173	159	152
Int32 + Int32 + C_3H_6	43	29	15	7

[a]See Figure 5; the letters t and s in parentheses stand for triplet and singlet electronic states, respectively. The energies in parentheses are spin-projected energies.

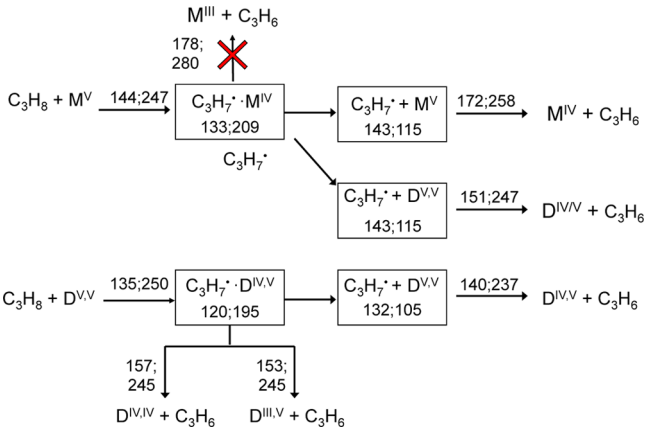

Figure 6. Possible reaction pathways for the first (left) and second (right) hydrogen abstractions in propane ODH on monomeric, M^V, and dimeric, $D^{V,V}$, vanadia sites on silica. The roman superscripts specify the oxidation state of the vanadium sites. The boxes designate intermediates, and the numbers next to the reaction arrow are energy barriers at 0 K and Gibbs free energy barriers (800 K) in kJ/mol.

Table 4. Comparison of Reaction Energies and Energy Barriers for Monomeric and Dimeric Vanadium Oxide Species on Silica

label	E_{el}	E_0	G_{600}	G_{800}
First H abstraction, V^{IV}				
Ts23 − Ts1	−9.2	−8.3	0.2	3.6
Ts23−2[a] − Ts1	−7.9	−8.0	−11.5	−12.6
Int22−1 − Int2	−12.7	−12.4	−3.6	−0.5
Int22−2[a] − Int2	−9.4	−9.4	−13.2	−14.2
Int32−1 − Int12	−12.0	−12.0	−11.0	−11.0
Second H abstraction, V^{III}				
Ts24−1 − Ts3	−26.3	−25.2	−31.6	−33.0
Int23 − Int4	−19.2	−20.0	−21.8	−22.5
Int24 − Int10	−14.9	−15.2	−10.7	−9.3
Second H abstraction, V^{IV}/V^{IV} dimer formed				
Ts27−1 − Ts17	−16.7	−15.4	−13.8	−13.1
Ts27−2 − Ts17	−14.0	−12.8	4.2	10.4
Int30−1 − Int14	−11.1	−11.6	−17.4	−19.6
Int30−2 − Int14	−6.0	−6.2	−13.9	−16.4
Int31−1 − Int12	−12.2	−12.2	−12.6	−12.7
Int31−2 − Int12	−3.1	−3.6	−22.2	−28.4
Second H abstraction, two V^V/V^{IV} dimers formed				
TS32−1 − Ts17	−35.0	−32.2	−24.4	−21.6
Int34−1 − Int14	−27.5	−27.8	−35.4	−38.0
Int32−1 − Int12	−23.6	−23.5	−20.9	−19.9

[a]Results for dimer-2 model.

Int2, Int23/Int4, Int30/Int14, and Int34/Int14. Intermediates that differ by desorption of the hydrocarbon species from the latter, namely, Int32/Int12, Int24/Int10, Int31/Int12, and Int32/Int12, respectively, are also shown in Table 4, and their energies also follow the changes of the barriers.

Whereas the energy barriers and reaction energies for all relevant steps are lower on dimeric sites than on monomeric sites, the Gibbs free energies show some exceptions. For the first H abstraction, G_T-E_0 makes a large positive contribution of about 9−12 kJ/mol to the Ts23−Ts1 and Int22−Int2 differences when dimer-1 is considered, but a negative contribution of about 4−5 kJ/mol when the dimer-2 model is considered. This indicates some sensitivity to the model used. The G_T-E_0 result is essentially the entropy term and largely determined by the conversion of three rotational and three

dx.doi.org/10.1021/ja503130z | J. Am. Chem. Soc. 2014, 136, 7751−7761

translational degrees of freedom of propane (in the reference structure Int0 + propane) into six low frequency vibrational modes of the propyl radical relative to the active surface site in the transition structures Ts23/Ts1 and the first intermediate Int22/Int2. Small errors in these low frequencies will have a large effect on the calculated G_T value. Moreover, the harmonic approximation (which is unavoidable for computational reasons) faces limits for these modes, in particular at high temperatures.

4.3. Microkinetic Simulations. To understand how different elementary steps couple into an overall reaction, we employed microkinetic modeling that includes Int0 to Int31, Ts1 to Ts31, propane, propene, water, propanol, as well as the propyl radical. Three different simulations are performed for surfaces with (a) monomeric sites only, (b) dimeric sites only, and (c) 50% monomeric and 50% dimeric sites.

Figure 7 shows the molar amount of gas phase species with progressing time on a logarithmic scale for cases (a) and (b),

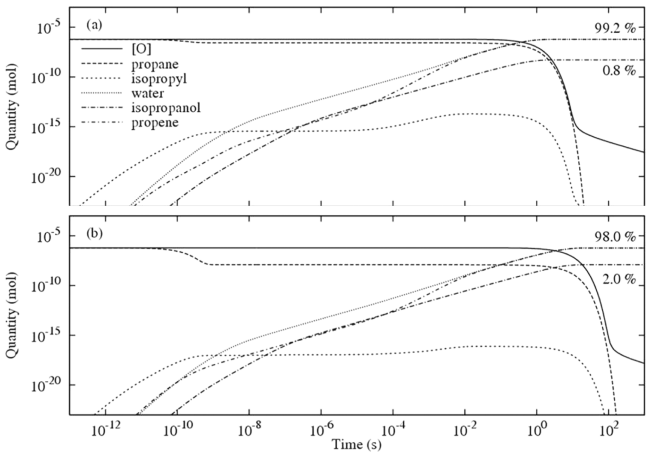

Figure 7. Microkinetic modeling of the reaction of propane on monomeric and dimeric silica supported vanadia under oxidizing atmosphere within the framework of a two-site mechanism (see text). Only gas phase species quantities are represented. (a) Monomeric species only. (b) Dimeric species only.

whereas Figure 8 shows the desorption flows of propene, isopropyl, and isopropanol for case (c). First, propane adsorbs on free vanadia sites, and the propane quantity in the gas phase decreases. Adsorption equilibrium is reached after around 1 ns.

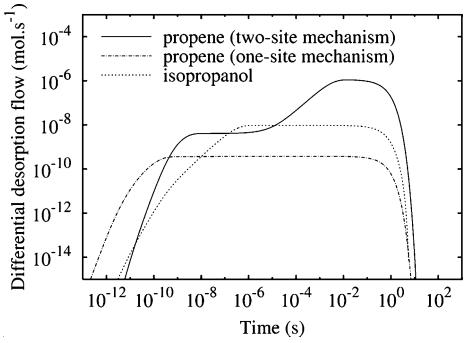

Figure 8. Microkinetic modeling of the reaction of propane on monomeric and dimeric silica supported vanadia under oxidizing atmosphere within the framework of a two-site mechanism (see text). Only differential adsorption flows of propene and isopropanol are here represented. Experimental conditions: see text.

Simultaneously, isopropyl, water, propene, and isopropanol start slowly to desorb. The most abundant species is isopropyl, followed by water, propene, and finally isopropanol. Water mostly results from the reoxidation of free V^{+IV} sites, which explains that its quantity growths more rapidly than that of propene. Figure 8 shows that at around 10 ns the desorption flow of isopropanol becomes larger than that of propene. Because the rate constant is smaller for desorption of isopropanol from Int7 than for propene from Int4 ($\Delta G_{600\ K}$ is +8 kJ/mol compared to −59 kJ/mol), Int7 first has to accumulate before isopropanol starts desorbing. However, as soon as the quantity of Int7 is stabilized, the relative desorption flows of isopropanol and propene reflect the fact that the rate constants of formation from Int2, is larger for Int7 than for Int4. At around 100 μs, the quantity of propene in the gas phase becomes suddenly much larger than that of isopropanol (note the logarithmic scale in Figure 7). The reason is that isopropyl radicals have adsorbed on V^{+V} sites during the previous period, and the "site cooperation" part of the mechanism (second hydrogen abstraction on a different V^{+V} site than the first) becomes more favorable than the one leading to isopropanol. The production of propene overcomes that of isopropanol as soon as the quantities of surface species that are involved in the "site cooperation" part of the mechanism are stabilized. At around 10 ms, the steady state catalytic regime is reached. The reaction ends after 10 s when propane is totally consumed.

The final partial pressures of gas phase species are listed in Table 5. Propene represents more than 99% of the reaction

Table 5. Final Quantities of Gas Phase Species Obtained by Microkinetic Modeling of the Reaction of Propane on Monomeric and Dimeric Silica Supported Vanadia under Oxidizing Atmosphere within the Framework of a Two-Site Mechanism (See Text)[a]

gas phase species	(a) pure monomer (kPa)	(b) mixture 50−50% (kPa)	(c) pure dimer (kPa)
water	39.67	39.41	39.21
isopropanol	0.33	0.59	0.79
propene	39.67	39.41	39.21

[a](a) Monomeric species only. (b) 50% monomeric species and 50% dimeric species. (c) Dimeric species only.

products at the end of the reaction, and isopropanol less than 1%. This is in agreement with the experimentally based suggestion that low propene selectivity mainly stems from propene oxidation and not from reactant and ODH intermediates oxidation.

The simulations discussed above concern one particular set of experimental parameters (see Section 3.2). To check whether the obtained reaction chronology corresponds to a general reaction scheme that is valid also for other experimental conditions, we performed additional simulations for cases (a), (b), and (c) above. We select propane pressures from 0 up to 60 kPa taken every 10 kPa, vanadia coverages from 0 up to 2 nm^{-2} taken every 0.5 nm^{-2}, and temperatures from 600 to 900 K taken every 50 K. In each case, the reaction chronology remains the same, and the final quantities of products vary by a few percent only when changing the experimental parameters. Temperatures below 200 K must be reached before any relevant change in the reaction chronology is observed.

dx.doi.org/10.1021/ja503130z | J. Am. Chem. Soc. 2014, 136, 7751−7761

To calculate the overall rate of the reaction, we consider the main reaction steps:

Int0 + propane → Int1, Ts1, Int2(tr /bs)
→ Int12 + propyl

Int0 + propyl → Int13, Ts18 to Ts19, Int14
→ Int12 + propene, Int16
→ Int17 + propene

Int20 + propane → Int21, Ts23, Int22(tr /bs)
→ Int32 + propyl

Int20 + propyl → Int33, Ts32 to Ts34, Int34
→ Int32 + propene, Int36
→ Int37 + propene

Figure 9 summarizes the reaction scheme. Reoxidation is not considered. Quantities of reactants (propane and vanadia sites)

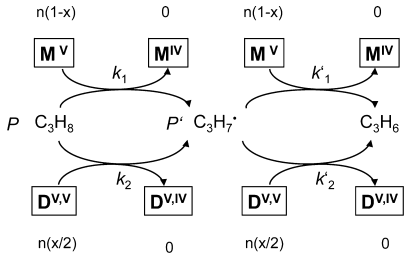

Figure 9. Two-site reaction scheme for the ODH of propane on a mixture of monomeric (M) and dimeric (D) vanadia species supported on silica. The Roman superscripts denote vanadium oxidation states. P and P' are pressures, and the top and bottom lines show the coverages that are used for modeling the system in the steady-state, x representing the fraction of vanadium atoms involved in dimeric species.

are kept constant. Quantities of products (propene and reduced vanadia sites) are kept zero. The overall steady state reaction flow is calculated for several sets of experimental parameters in the following range: $P_{propane}$ = 0−60 kPa, $n_{vanadia}$ = 0−2 nm^{-2}, T = 600−900 K. The overall reaction flow F is found to depend linearly on $P_{propane}$ and $n_{vanadia}$,

$$F = k(P_{propane}/P^{\circ})(n_{vanadia}/n^{\circ}) \quad (1)$$

where P° is the standard pressure (1 bar), n° the reference coverage (1 mol m^{-2}, i.e., 6.022 × 10^5 nm^{-2}), and k the rate constant of the overall reaction. The Arrhenius activation energy is evaluated as numerical derivative of the logarithm of the overall rate constant with respect to the temperature (see Supporting Information).

The rate constants, Arrhenius activation energies, and prefactors are given in Table 6 for 600, 750, and 900 K. For dimeric sites the activation barriers are lower, and the rate constants are larger than for monomeric sites. Hence, the conversion of propane into isopropyl and subsequently propene preferentially occurs on a dimeric site (Table 6). For monomeric and dimeric sites, Ts1 and Ts23, respectively, are the only transition structures that have an influence on the rate constants with a relative variation of −16 and −32% mol kJ^{-1}, respectively, at 750 K (1% mol kJ^{-1} means that the rate constant changes by 1% when the energy barrier changes by 1 kJ mol^{-1}). These are rate-determining steps even if their Gibbs free energies are lower than that of the subsequent transition states. The reaction flow and the rate constant are determined by the kinetics of the first reaction step because isopropyl is a gas phase intermediate. The further reaction steps only influence the stationary isopropyl pressure. In our previous study on monomeric sites we have already pointed out that this is due to assuming fast reoxidation so that the ratio of reduced sited to nonreduced sites is small.[26] Experiments for MoO_x/ZrO_2 catalysts have also shown that H-abstraction is an irreversible step, and not an equilibrium.[51] When feeding a 1:1 mixture of C_3H_8 and C_3D_8, no scrambling has been observed, which would be expected if there was an equilibrium between propane and propyl.

For vanadium oxide catalysts on silica (<3 V nm^{-2}) a turnover frequency (TOF) of 0.003 $mol_{C_3H_8}/mol_V$ s has been measured at 623 K.[8] Concomitantly with the higher temperature of 773 K, on differently structures silica supports (MCM-41, MCM-48, SBA-15, amorphous SiO_2) with coverages of 0.4−1.4 V nm^{-2} similar turnover frequencies of 0.010−0.016 $mol_{C_3H_8}/mol_V$ s have been measured. The variation of these TOFs across the different supports is only slightly larger than the estimated uncertainty of an individual measurement, which justifies the use of our silsesquioxane model as generic model for silica surfaces in general. The apparent Arrhenius activation energies were 97−112 kJ/mol.[52] Similar results have been reported for propene formation from propane over differently loaded VOx/MCM-41 materials at 748 K ($C_3H_8/O_2/N_2$ = 40/20/40).[25] From the data in Figure 9a of the latter article, the following values are obtained (V loading in parentheses): 128

Table 6. Overall Rate Constants, k (mol/s), Arrhenius Activation Energy, E_a (kJ/mol), and Prefactor, A (mol/s), at Different Temperatures, T (K), for the Formation of Isopropyl Radical and V^{+IV} Sites from Propane and V^{+V} Sites (R1) and the Formation of Propene and V^{+IV} Sites from Isopropyl and V^{+V} Sites (R2) on Monomeric and Dimeric Vanadia Sites on Silica Support

		monomer			dimer		
	T	E_a	A	k_1	E_a	A	k_2
R1	600	120.6	1.95 × 10^9	6.18 × 10^{-2}	109.7	8.55 × 10^8	2.40 × 10^{-1}
	750	124.0	3.54 × 10^9	8.25 × 10^0	113.7	1.74 × 10^9	2.10 × 10^1
	900	127.8	6.20 × 10^9	2.37 × 10^2	117.7	3.14 × 10^9	4.61 × 10^2
R2	600	−4.6	4.77 × 10^7	1.19 × 10^8	−19.0	1.61 × 10^8	7.18 × 10^9
	750	0.1	1.11 × 10^8	1.09 × 10^8	−20.9	1.10 × 10^8	3.14 × 10^9
	900	4.1	1.99 × 10^8	1.15 × 10^8	−18.1	1.66 × 10^8	1.86 × 10^9

dx.doi.org/10.1021/ja503130z | J. Am. Chem. Soc. 2014, 136, 7751−7761

(0.6 wt %), 109 (1.2 wt %), and 104 kJ/mol (2.7 wt %), which are in as good agreement with the calculated values for 750 K, 124 and 114 kJ/mol for monomeric and dimeric sites, respectively, as one can expect for B3LYP calculations, given the limited accuracy of DFT in general and of the B3LYP functional in particular.[53]

For catalysts with vanadium loadings of up to 5.3 wt % (V surface density below 1 V nm^{-2}) the TOF values are nearly constant, however within error bars of 20%.[25] Nearly constant TOF values (0.3×10^{-3} s^{-1}[8] at 623 K) have also been observed for vanadium coverages between 1.5 and 2.6 V/nm.[28] For a mixture of monomer and dimer species with a fraction x of vanadium atoms being part of dimers, the total rate constant is given by

$$k(x) = (1 - x)k_1 + (x/2)k_2$$

From the monomer and dimer rate constants in Table 6, k_1 and k_2, respectively, we find that for $x = 0.5$ the total rate constant increases by 14% at 750 K, well within the uncertainty of the experimental values. We conclude that our results are compatible with the known experimental information.

4.4. Polymeric Vanadium Oxide Species and Their Reactivity. To estimate the activity of oligomeric vanadium oxide species beyond dimeric species, we calculate reaction energies for the oxidative dehydrogenation of propane by silsesquioxane models in which an increasing number of Si−H groups is replaced by vanadyl groups. The composition of the cluster models is $(OV)_nSi_{8-n}O_{12}H_{8-n}$. For models with $n = 2$, 3, and 4, oligomeric vanadium oxide species of size n and all possible combinations of smaller species are considered. Figure 6 shows the different distribution of vanadium oxide species and their relative energies. There is a very small preference for the polymers of higher order. For instance, the energy of formation of a dimeric vanadium oxide species ($(OV)_2Si_6O_{12}H_6$) and a pure silica model ($Si_8O_{12}H_8$) from two monomeric species ($OVSi_7O_{12}H_7$) is 1 kJ/mol. The energy of the "true" dimer, V2(2), is only 1 to 3 kJ/mol lower than that of the isomers with two monomeric sites, V2(2 × 1)a and V2(2 × 1)b (Figure 10). This implies that the distribution of $O{=}V(O-)_3$ species on a silica surface is largely statistical from the thermodynamic point of view.

The microkinetic modeling (Section 4.3) has shown that the first hydrogen abstraction is rate limiting, and in Section 4.2 evidence has been produced that the change in the energy barrier follows the change in the energy of the reaction (Table 4)

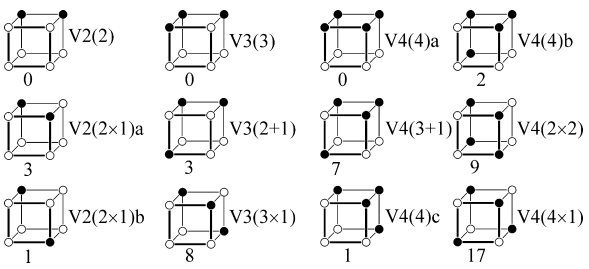

Figure 10. Relative stability of vanadyl-exchanged silsesquioxanes with different patterns for 2, 3, and 4 O═V/H—Si substitutions (left to right). Dark and white balls are vanadyl and H−Si, respectively. The bridging oxygen atoms are not shown. The numbers are electronic energies in kJ/mol.

$$(OV)_nSi_{8-n}O_{12}H_{8-n} + C_3H_8 \rightarrow (HOV^{IV})(OV)_{n-1}Si_{8-n}O_{12}H_{8-n} + C_3H_7^{\bullet} \quad (2)$$

Table 7 shows that the energies and Gibbs free energies of reaction 2 decrease with increasing size of the vanadia cluster (n = 1−4, 8). With 12 kJ/mol the decrease is largest for the step n = 1 to n = 2 (see Int32−1 − Int12 in Table 4). The changes of the Gibbs free energies are dominated by the changes of the reaction energies. We conclude that the decrease of the energy barriers for the ODP reaction when passing from monomeric to dimeric sites continues when passing to trimeric, tetrameric, and even larger sites.

Table 7. Energies and Gibbs Free Energies for the Reaction $(OV)_n(HSi)_{8-n}O_{12}$ + Propane → $HOV(OV)_n(HSi)_{8-n}O_{12}$ + Propyl[a]

species (n)		ΔE_0	ΔG_{600}	ΔG_{800}
monomer (1)	1	160	138	125
dimer (2)	2	148	127	114
trimer (3)	3	143	122	109
tetramer (4)	4	139	121	107
octamer (8)	8	132	110	98

[a] ΔE_0 and ΔG_T are reaction energies at 0 K and Gibbs free reaction energies at T K in kJ/mol. In all cases the zero-point vibrational energy contribution to the reaction energy is zero, i.e., $\Delta E_{el} = \Delta E_0$.

In the overall oxidative dehydrogenation, two hydrogen atoms of propane are transferred to the catalyst. We have shown above and also in the literature[26] that vanadyl oxygen atoms are the most active in hydrogen abstraction. The two hydrogen atoms can be transferred to two different vanadyl oxygen atoms yielding two $HOV^{IV}(d^1)$ sites, or to the same atom yielding a $H_2O{\cdot}V^{III}(d^2)$ site. Hence, we consider the reactions

$$(OV)_nSi_{8-n}O_{12}H_{8-n} + C_3H_8 \rightarrow (HOV^{IV})_2(OV)_{n-2}Si_{8-n}O_{12}H_{8-n} + C_3H_6 \quad (3a)$$

and

$$(OV)_nSi_{8-n}O_{12}H_{8-n} + C_3H_8 \rightarrow H_2O{\cdot}V^{III}(OV)_{n-1}Si_{8-n}O_{12}H_{8-n} + C_3H_6 \quad (3b)$$

Figure 11 shows the energies for these reactions as a function of the size m of the "true" or "linked" oligomeric vanadium oxide species that can occur in all $(OV)_nSi_{8-n}O_{12}H_{8-n}$ models with $n \geq m$. Indeed, as Figure 10 shows, monomeric species occur in all models from n = 1 to n = 4, whereas dimers occur in models with n = 2 to n = 4.

The energies for both reactions 3a and 3b decrease almost linearly with the oligomer size m, but there is also a dependency on the total vanadium oxide content of the $(OV)_nSi_{8-n}O_{12}H_{8-n}$ model. In Section 4.3, we showed that the energy barriers follow the same trend as the reaction energies. Here we provide additional evidence for an increase of reactivity with increasing size of the vanadia species.

The energies are around 35 kJ/mol lower when two $HOV^{IV}(d^1)$ sites are formed 3a instead of one $H_2O{\cdot}V^{III}(d^2)$ site 3b. This means that the redox disproportionation

$$2V^{IV}(d^1) \rightarrow V^{V}(d^0) + V^{III}(d^2)$$

dx.doi.org/10.1021/ja503130z | J. Am. Chem. Soc. 2014, 136, 7751−7761

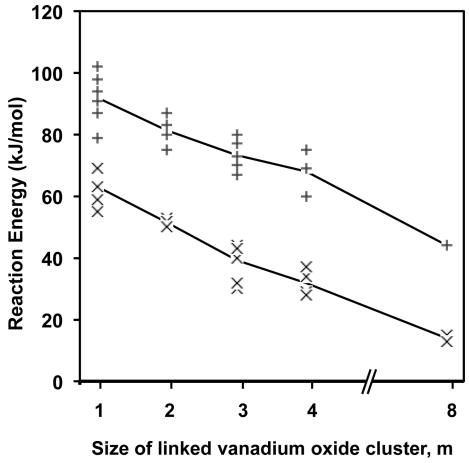

Figure 11. B3LYP energies (kJ/mol) of reactions 3a (x) and 3b (+) as a function of the size m of $(VO_{2.5})_m$ linked clusters in $V_nSi_{8-n}O_{12+n}H_{8-n}$ silsesquioxane models. For n = 1 and 2 the structures are shown in Figure 1a,b, respectively. All O═V/H—Si substitution patterns and H attachments are considered (Figure 10). The solid line connects the average values for a given linked clusters size m in all possible silsesquioxane models ($n \geq m$). The energy for the formation of 2 $HOV^{IV}(d^1)$ species is determined using two clusters.

is endothermic for the vanadium oxide species studied here. Indeed, the standard heats of formation for solid V_2O_5, V_2O_4, and V_2O_3 (−1551, −1427, and −1219 kJ/mol, respectively[54]) yield for the reaction

$$V_2O_{4(s)} \rightarrow \frac{1}{2}V_2O_{5(s)} + \frac{1}{2}V_2O_{3(s)}$$

a standard enthalpy of 42 kJ/mol (T = 298 K, p = 1 atm), whereas the present study yields for the reactions

$$2HOV^{IV}(OV)Si_7O_{12}H_7 \rightarrow H_2O{\cdot}V^{III}Si_7O_{12}H_7 + OV^{V}Si_7O_{12}H_7$$

and

$$(HOV^{IV})_2Si_6O_{12}H_6 \rightarrow H_2O{\cdot}V^{III}(OV)Si_6O_{12}H_6$$

standard enthalpies of 40 and 50 kJ/mol, respectively.

As a further step toward a reactivity descriptor, eqs 3a and 3b may be decomposed into the oxidation of the substrate:

$$C_3H_8 + \frac{1}{2}O_2 \rightarrow C_3H_6 + H_2O \quad (4)$$

and reduction of the vanadium oxide species yielding an oxygen defect site:

$$O = V^{V}(O-)_3 \rightarrow V^{III}(O-)_3 + \frac{1}{2}O_2 \quad (5)$$

Reaction 5 describes formation of a vanadyl oxygen defect or dissociation of the vanadyl bond. This reaction energy has been used before to discuss the reactivity differences between different vanadium oxide species.[35,55,56] The energy of reaction 3b decreases from 102 to 87 and to 50 kJ/mol when passing from monomeric (n = 1) to true dimeric (n = 2), and to octameric (n = 8) species, respectively, while the energy of reaction 5 changes from 287 to 277 and to 256 kJ/mol, respectively.[35] The parallel trend confirms that the vanadyl bond dissociation energy (eq 5) is a descriptor of the reactivity of vanadium oxide species in oxidation reactions.

Comparison with vanadyl bond dissociation energies calculated for monomeric, dimeric, and oligomeric vanadia species on the nonreducible zirconia[57] and alumina[58,59] supports indicate that changes of the particle size may cause activity changes of the same order of magnitude as changes of the support.

5. CONCLUSIONS

We find that the size-distribution of oligomeric vanadium oxide species on silica support is largely statistical with a very small energetic preference for larger oligomers. At submonolayer coverage, a mixture of monomeric, dimeric, and oligomeric species is likely to exist.

For monomeric and dimeric vanadium oxide species supported on silica, we have examined the reaction pathways of the oxidative dehydrogenation of propane in detail. The first step is hydrogen abstraction by a vanadyl group yielding a biradicaloid intermediate that consists of a propyl radical attached to a HOV^{IV} site. The second hydrogen abstraction toward propene can occur at the same site yielding $H_2O{\cdot}V^{III}$ or at a fresh, "unreacted" site, yielding two HOV^{IV} species. The second route always has lower barriers and leads to more stable products. We conclude that the catalytic cycle is more likely to feature a $V^{V}(d^0)/V^{IV}(d^1)$ than a $V^{V}(d^0)/V^{III}(d^2)$ redox couple. In both routes direct propene formation competes with an indirect route via surface alkoxides or surface alcohols. Our microkinetic simulations show that in the stationary state the amount of isopropanol is less than 1% of the products.

Our microkinetic simulations for the oxidative dehydrogenation of propane on a mixture of monomeric and dimeric vanadia species supported on silica show that the first hydrogen abstraction is rate-determining. This is due to the fast reoxidation of the vanadia catalyst. Even if subsequent transition states have lower Gibbs free energies than the initial H atom transfer, the further reaction steps only influence the stationary isopropyl pressure, which turns out to be exceedingly small.

The microkinetic simulations have further shown that for dimeric sites the activation barriers are about 10 kJ/mol lower than for monomeric sites. The simulated Arrhenius activation barrier (124 and 114 kJ/mol at 750 K) are in the same range as experimental values (104−128 kJ/mol).[25] If 50% of the vanadium atoms are present as dimers the rate constant increases by only 14% (750 K), well within the uncertainty limits.[25]

For the energy barriers of the rate-determining first H atom transfer step, we have calculated about 10 kJ/mol smaller values for dimers than for monomers. In accord with the Evans−Polanyi relation, this was accompanied by a similar change for the reaction energies. Using the reaction energy as a reactivity descriptor, we conclude that the decrease of the energy barriers for the ODP reaction with the vanadia cluster size continues when passing from dimers to larger oligomers.

Together with an almost statistical size distribution for submonolayer coverage and the fewer number of oligomeric species per vanadium atom, this would be compatible with the observed almost constant turnover frequencies for vanadia loadings of a few V atoms per nm^2.[8,25]

We note that our conclusions apply specifically to vanadia supported on silica. For vanadia supported on ceria the opposite has been found: the activity decreases with larger

dx.doi.org/10.1021/ja503130z | J. Am. Chem. Soc. 2014, 136, 7751−7761

particles size, with the monomer being the most active species.[56,60] Moreover, differently from silica, on the ceria support there is an energetic preference for larger species.[60,61]

■ ASSOCIATED CONTENT

Supporting Information

Data used in the microkinetic simulation and detailed formulas used for transition state theory and statistical thermodynamics. This material is available free of charge via the Internet at http://pubs.acs.org.

■ AUTHOR INFORMATION

Corresponding Author

js@chemie.hu-berlin.de

Notes

The authors declare no competing financial interest.

■ ACKNOWLEDGMENTS

This work has been supported by an Alexander von Humboldt fellowship for XR and by "Deutsche Forschungsgemeinschaft (Sonderforschungsbereich 546)". We thank E. V. Kondratenko for providing the Arrhenius activation energies from the data in Figure 9a of ref 25.

■ REFERENCES

(1) Blasco, T.; Lopez Nieto, J. M. *Appl. Catal., A* **1997**, *157*, 117.
(2) Weckhuysen, B. M.; Keller, D. E. *Catal. Today* **2003**, *78*, 25.
(3) Chen, K.; Bell, A. T.; Iglesia, E. *J. Catal.* **2002**, *209*, 35.
(4) Albonetti, S.; Cavani, F.; Trifiro, F. *Catal. Rev.: Sci. Eng.* **1996**, *38*, 413.
(5) Olthof, B.; Khodakov, A.; Bell, A. T.; Iglesia, E. *J. Phys. Chem. B* **2000**, *104*, 1516.
(6) Argyle, M. D.; Chen, K.; Bell, A. T.; Iglesia, E. *J. Catal.* **2002**, *208*, 139.
(7) Magg, N.; Immaraporn, B.; Giorgi, J. B.; Schroeder, T.; Bäumer, M.; Döbler, J.; Wu, Z.; Kondratenko, E.; Cherian, M.; Baerns, M.; Stair, P. C.; Sauer, J.; Freund, H.-J. *J. Catal.* **2004**, *226*, 88.
(8) Tian, H.; Ross, E. I.; Wachs, I. E. *J. Phys. Chem. B* **2006**, *110*, 9593.
(9) Wachs, I. E. *Dalton Trans.* **2013**, *42*, 11762.
(10) Wu, Z. L.; Dai, S.; Overbury, S. H. *J. Phys. Chem. C* **2010**, *114*, 412.
(11) Cavalleri, M.; Hermann, K.; Knop-Gericke, A.; Hävecker, M.; Herbert, R.; Hess, C.; Oestereich, A.; Döbler, J.; Schlögl, R. *J. Catal.* **2009**, *262*, 215.
(12) Argyle, M. D.; Chen, K.; Resini, C.; Krebs, C.; Bell, A. T.; Iglesia, E. *J. Phys. Chem. B* **2004**, *108*, 2345.
(13) Venuto, P. B. *Microporous Mater.* **1994**, *2*, 297.
(14) Cullis, C. F. *Ind. Eng. Chem.* **1967**, *59*, 19.
(15) Kogan, S. B.; Schramm, H.; Herskowitz, M. *Appl. Catal., A* **2001**, *208*, 185.
(16) Batiot, C.; Hodnett, B. K. *Appl. Catal., A* **1996**, *137*, 179.
(17) Limberg, C. *Angew. Chem., Int. Ed.* **2003**, *42*, 5932.
(18) Shaik, S.; Visser, S. P. d.; Ogliaro, F.; Schwarz, H.; Schröder, D. *Curr. Opin. Chem. Biol.* **2002**, *6*, 556.
(19) Feyel, S.; Schröder, D.; Rozanska, X.; Sauer, J.; Schwarz, H. *Angew. Chem., Int. Ed.* **2006**, *45*, 4677.
(20) Feyel, S.; Döbler, J.; Schröder, D.; Sauer, J.; Schwarz, H. *Angew. Chem., Int. Ed.* **2006**, *45*, 4681.
(21) Schlögl, R. *Top. Catal.* **2011**, *54*, 627.
(22) Khodakov, A.; Olthof, B.; Bell, A. T.; Iglesia, E. *J. Catal.* **1999**, *181*, 205.
(23) Oyama, S. T.; Somorjai, G. A. *J. Phys. Chem.* **1990**, *94*, 5022.
(24) Oyama, S. T. *J. Catal.* **1991**, *128*, 210.
(25) Kondratenko, E.; Cherian, M.; Baerns, M.; Su, D.; Schlögl, R.; Wang, X.; Wachs, I. E. *J. Catal.* **2005**, *234*, 131.
(26) Rozanska, X.; Fortrie, R.; Sauer, J. *J. Phys. Chem. C* **2007**, *111*, 6041.
(27) Fu, H.; Liu, Z.-P.; Li, Z.-H.; Wang, W.-N.; Fan, K.-N. *J. Am. Chem. Soc.* **2006**, *128*, 11114.
(28) Dai, G. L.; Li, Z. H.; Lu, J.; Wang, W. N.; Fan, K. N. *J. Phys. Chem. C* **2012**, *116*, 807.
(29) Redfern, P. C.; Zapol, P.; Sternberg, M.; Adiga, S. P.; Zygmunt, S. A.; Curtiss, L. A. *J. Phys. Chem. B* **2006**, *110*, 8363.
(30) Cheng, M.-J.; Chenoweth, K.; Oxgaard, J.; Duin, A. v.; Goddard, W. A., III *J. Phys. Chem. C* **2007**, *111*, 5115.
(31) Wannakao, S.; Boekfa, B.; Khongpracha, P.; Probst, M.; Limtrakul, J. *ChemPhysChem* **2010**, *11*, 3432.
(32) Alexopoulos, K.; Reyniers, M.-F.; Marin, G. B. *J. Catal.* **2012**, *289*, 127.
(33) Cheng, L.; Ferguson, G. A.; Zygmunt, S. A.; Curtiss, L. A. *J. Catal.* **2013**, *302*, 31.
(34) Döbler, J.; Pritzsche, M.; Sauer, J. *J. Am. Chem. Soc.* **2005**, *127*, 10861.
(35) Sauer, J.; Döbler, J. *Dalton Trans.* **2004**, *19*, 3116.
(36) Vyboishchikov, S. F.; Sauer, J. *J. Phys. Chem. A* **2001**, *105*, 8588.
(37) Asmis, K. R.; Santambrogio, G.; Brümmer, M.; Sauer, J. *Angew. Chem.* **2005**, *117*, 3182.
(38) Becke, A. D. *J. Chem. Phys.* **1993**, *98*, 5648.
(39) Schäfer, A.; Huber, C.; Ahlrichs, R. *J. Chem. Phys.* **1994**, *100*, 5829.
(40) Ahlrichs, R.; Bär, M.; Häser, M.; Horn, H.; Kölmel, C. *Chem. Phys. Lett.* **1989**, *162*, 165.
(41) Treutler, O.; Ahlrichs, R. *J. Chem. Phys.* **1995**, *102*, 346.
(42) Noodleman, L. *J. Chem. Phys.* **1981**, *74*, 5737.
(43) Caballol, R.; Castell, O.; Illas, F.; de P. R. Moreira, I.; Malrieu, J. P. *J. Phys. Chem. A* **1997**, *101*, 7860.
(44) Deglmann, P.; Furche, F.; Ahlrichs, R. *Chem. Phys. Lett.* **2002**, *362*, 511.
(45) Rozanska, X.; Kondratenko, E. V.; Sauer, J. *J. Catal.* **2007**, *256*, 84.
(46) Kämper, A.; Auroux, A.; Baerns, M. *Phys. Chem. Chem. Phys.* **2000**, *2*, 1069.
(47) *Mathematica*, version 5.2; Wolfram Research, Inc.: Champaign, IL, 2005.
(48) d^1 and d^2 mean that the nonbonding d-states at the vanadium atom are occupied with one and two electrons, respectively. This information is obtained by inspection of the natural orbitals with an occupation of one.
(49) Wesolowski, T. A.; Parisel, O.; Ellinger, Y.; Weber, J. *J. Phys. Chem. A* **1997**, *101*, 7818.
(50) Evans, M. G.; Polanyi, N. P. *Trans. Faraday Soc.* **1938**, *34*, 11.
(51) Chen, K. D.; Iglesia, E.; Bell, A. T. *J. Phys. Chem. B* **2001**, *105*, 646.
(52) Ovsitser, O.; Cherian, M.; Kondratenko, E. *J. Phys. Chem. C* **2007**, *111*, 8594.
(53) Zhao, Y.; Truhlar, D. G. *J. Phys. Chem. A* **2005**, *109*, 5656.
(54) D'Ans-Lax. In *Taschenbuch fuer Chemiker und Physiker*; Blachnik, R., Ed.; Springer Verlag: Berlin, 1998; Vol. 3, p 790.
(55) Todorova, T. K.; Ganduglia-Pirovano, M. V.; Sauer, J. *J. Phys. Chem. B* **2005**, *109*, 23523.
(56) Ganduglia-Pirovano, M. V.; Popa, C.; Sauer, J.; Abbott, H. L.; Uhl, A.; Baron, M.; Stacchiola, D.; Bondarchuk, O.; Shaikhutdinov, S.; Freund, H.-J. *J. Am. Chem. Soc.* **2010**, *132*, 2345.
(57) Hofmann, A.; Ganduglia-Pirovano, M. V.; Sauer, J. *J. Phys. Chem. C* **2009**, *113*, 18191.
(58) Brázdová, V.; Ganduglia-Pirovano, M. V.; Sauer, J. *J. Phys. Chem. C* **2010**, *114*, 4983.
(59) Beck, B.; Harth, M.; Hamilton, N. G.; Carrero, C.; Uhlrich, J. J.; Trunschke, A.; Shaikhutdinov, S.; Schubert, H.; Freund, H.-J.; Schlögl, R.; Sauer, J.; Schomäcker, R. *J. Catal.* **2012**, *296*, 120.
(60) Penschke, C.; Paier, J.; Sauer, J. *J. Phys. Chem. C* **2013**, *117*, 5274.
(61) Paier, J.; Kropp, T.; Penschke, C.; Sauer, J. *Faraday Discuss.* **2013**, *162*, 233.